

Structural and chemical embrittlement of grain boundaries by impurities: a general theory and first principles calculations for copper

A. Y. Lozovoi, A. T. Paxton, and M. W. Finnis*

*Atomistic Simulation Centre, School of Mathematics and Physics,
Queen's University Belfast, Belfast BT7 1NN, Northern Ireland, U.K.*

(Dated: May 25, 2019)

First principles calculations of the $\Sigma 5(310)[001]$ symmetric tilt grain boundary in Cu with Bi, Na, and Ag substitutional impurities provide evidence that in the phenomenon of Bi embrittlement of Cu grain boundaries electronic effects do not play a major role; on the contrary, the embrittlement is mostly a structural or “size” effect. Na is predicted to be nearly as good an embrittler as Bi, whereas Ag does not embrittle the boundary in agreement with experiment. While we reject the prevailing view that “electronic” effects (*i.e.*, charge transfer) are responsible for embrittlement, we do not exclude the rôle of chemistry. However numerical results show a striking equivalence between the alkali metal Na and the semi metal Bi, small differences being accounted for by their contrasting “size” and “softness” (defined here). In order to separate structural and chemical effects unambiguously if not uniquely, we model the embrittlement process by taking the system of grain boundary and free surfaces through a sequence of precisely defined *gedanken* processes; each of these representing a putative mechanism. We thereby identify *three* mechanisms of embrittlement by substitutional impurities, two of which survive in the case of embrittlement or cohesion enhancement by interstitials. Two of the three are purely structural and the third contains both structural and chemical elements that by their very nature cannot be further unravelled. We are able to take the systems we study through each of these stages by explicit computer simulations and assess the contribution of each to the nett reduction in intergranular cohesion. The conclusion we reach is that embrittlement by both Bi and Na is almost exclusively structural in origin; that is, the embrittlement is a size effect.

PACS numbers: 61.72.Bb, 05.70.Np, 61.72.Mm, 68.35.Dv

Introduction

Impurity induced embrittlement of metals is an age old phenomenon. For the case of bismuth in copper, it was apparently first recorded in the scientific literature in the 1870s,¹ becoming a matter of both manufacturing importance and scientific curiosity in the 20th century. As far as we know the suggestion that segregation to grain boundaries was the culprit was first made by Cyril S. Smith in a comment to a paper in 1929² and this explanation is now generally accepted as the truth. Perhaps the most dramatic event resulting from grain boundary segregation embrittlement was the failure of the Hinkley Point ‘A’ nuclear reactor in 1969.^{3,4} Given that fast, brittle failure is a result of the segregation of insoluble impurities to grain boundaries, the physical, microscopic origin of the loss of cohesion is still a matter of intense debate and controversy. And origins may indeed be different for different metal and impurity combinations. At issue is the question, how can impurities segregated to grain boundaries at concentrations of a monolayer (ML) or less result in reduction in fracture toughness amounting to a ductile to brittle transition?

Opinions are currently divided into two schools of thought depending on whether it is believed that changes in the chemical bonding *between host atoms* due to the presence of impurities in their neighbourhood is the cause of the embrittlement. The alternative to such *electronic* mechanisms can loosely be described as a *size effect*.^{5,6,7} The electronic mechanisms of grain boundary embrittle-

ment can in turn be divided into grain boundary weakening and grain boundary stiffening arguments. In the former, the impurities withdraw some electronic charge from neighbouring host atoms which makes their cohesion across the boundary less strong.⁸ In the latter, the impurity presence at the boundary leads to the formation of strong directional bonds which make it more difficult for dislocations to glide during decohesion. This leads to local stress piling up in the vicinity of the grain boundary, and the crystal falls apart in a brittle manner.^{9,10,11}

The other group of mechanisms, in which the effects of electronic charge redistribution do not play a decisive role, has been relatively little studied.¹² As we have recently argued,¹³ the well known effect of the embrittlement of grain boundaries in copper by bismuth is a perfect illustration of such embrittlement. Very briefly our arguments were supported by three independent pieces of evidence obtained during a study of the $\Sigma 19a(331)[\bar{1}10]$ symmetric tilt grain boundary with segregated Bi. Firstly, the electronic structure showed no evidence of the “white line” in the electron energy loss near edge structure (ELNES) reported experimentally to support the charge transfer principle. (The existence of the white line has also been called into question on experimental grounds.¹⁴) Secondly, elastic constants of bulk Cu with impurities (Bi or Pb) strongly depend on volume, but not on the presence of the impurity. Thirdly, a Kanzaki analysis is consistent with a *central force* model of Cu–Bi bonding, in which case the ease of dislocation emission from a crack tip should not be affected by the

presence of Bi.

An opposite view was simultaneously expressed by Duscher *et al.*,¹⁵ according to whom the role of Bi at a grain boundary is to *donate* some of its electronic charge to the neighbouring copper atoms rendering them “zinc like” and resulting in the weakening of the Cu–Cu bonds across the boundary. This point of view then falls into the class of electronic mechanisms. Their conclusion was based on a study of the $\Sigma 5(310)[001]$ symmetric tilt grain boundary with an areal density of Bi atoms of 2.9 nm^{-2} (approximately 0.25 ML of Bi at the grain boundary plane). Evidence of charge transfer between Bi and Cu taking place was based upon experimental ELNES spectra. In addition, the authors of ref. [15] mention that the calculated Bi induced expansion of the grain boundary is far too small to be the reason for the grain boundary becoming weak if a “size effect” argument were correct. On the other hand, our recent arguments to support a size effect included the finding of a large grain boundary expansion at the $\Sigma 19a$ Bi segregated grain boundary.¹³

We decided to address the controversy further by turning to the the $\Sigma 5$ copper grain boundary so as to make a direct comparison with the conclusions of Duscher *et al.*¹⁵ Our theoretical calculations presented for the first time here, arrive at a very different conclusion. The grain boundary expansion turns out to be larger in our study and we contend that the grain boundary studied in ref. [15] *was not embrittled*—indeed these authors did not test this point either experimentally or theoretically. We find that at least one monolayer of Bi at this grain boundary is needed for embrittlement. Under those circumstances the $\Sigma 5$ grain boundary is particularly susceptible to Bi embrittlement.¹⁶ Comparison of the effect of Bi with that of Na and Ag provide further support for the principle that in the weakening of Cu grain boundaries by Bi, charge redistribution plays a negligible role.

More importantly, in this paper we suggest a unified approach within which the effects of an impurity can be split into those related to mechanical distortion and to chemical identities of impurity and host atoms. We then proceed with our *ab initio* data to demonstrate how these combine together to explain the deterioration of grain boundary cohesion for purely structural reasons.

The structure of this paper is as follows. We briefly summarise the connection between fracture mechanics and thermodynamics of decohesion in section I, in order to make clear how the quantities we calculate relate to fracture toughness. Section II offers a general approach as to how the various contributions which weaken or strengthen a given boundary can be quantified using explicit calculation of the changes in total energy during the stages of a thought experiment. Technical details of the calculations, parameters used and tests of the method are described in section III. We present our results for the pure Cu grain boundary and grain boundaries segregated with Bi, Na and Ag in sections IV, V and VI. Section VII aims to identify the dominant mechanism responsible for grain boundary embrittlement by Bi and

Na in terms of size, stiffness and chemical properties of the impurity atoms. The section follows the method outlined in section II. Our conclusions may be found in section VIII.

I. THERMODYNAMICS OF GRAIN BOUNDARY EMBRITTLEMENT AND RELATION TO TOTAL ENERGY IN ELECTRONIC STRUCTURE CALCULATIONS

Grain boundary decohesion is a complex process involving propagation of a crack under load and possibly simultaneous emission of lattice or partial dislocations. Its proper description requires atomistic simulations at the mesoscopic level which is out of the reach of *ab initio* techniques. The approach that makes the problem manageable is due to Rice, Thomson and Wang.^{17,18} An atomically sharp crack at a grain boundary will advance either in brittle or ductile fashion depending on whether the minimal energy per unit area of crack advance (energy release rate) required to emit a single dislocation, $\mathcal{G}_{\text{disl}}$, is higher or lower than the energy release rate associated with brittle cleavage of the crystal along the grain boundary, $\mathcal{G}_{\text{cleav}}$.^{17,19} If $\mathcal{G}_{\text{cleav}} < \mathcal{G}_{\text{disl}}$, the crack remains atomically sharp during decohesion which is therefore brittle, otherwise the system begins to emit dislocations which blunt the crack. In practice, $\mathcal{G}_{\text{disl}}$ can be accessed through the anisotropic theory of crystal defects; for typical, pure Cu grain boundaries, $\mathcal{G}_{\text{disl}}$ falls in the region $1\text{--}2 \text{ J/m}^2$ (ref. [20]). Our task is thereby reduced to determining whether segregation may reduce $\mathcal{G}_{\text{cleav}}$ to a value significantly lower than this, hence triggering a ductile to brittle transition.

As regards $\mathcal{G}_{\text{cleav}}$, in the limit of perfectly elastic brittle fracture, neglecting lattice trapping and energy dissipation through phonon emission, it represents the reversible work needed to convert unit area of grain boundary into twice that area of free surface. The analysis is greatly complicated by impurity segregation compared to fracture in pure materials. This is because, whereas it may be taken that the impurity at the grain boundary prior to fracture is in equilibrium with that in the adjoining crystals, having an excess concentration Γ_{gb} per unit area, the concentration profile at the surface cannot generally be predicted *a priori*. As pointed out by Seah,⁵ and by Hirth and Rice²¹ one may imagine two limiting cases. In the first we suppose that the growth of the crack is slow compared to the rate of concentration equilibration between the surfaces produced and their underlying bulk. In that case the grain boundary and surface excess concentrations of impurity are at all times in accord with the equilibrium adsorption isotherms and depend only on the temperature and bulk concentrations, and we identify $\mathcal{G}_{\text{cleav}}$ with the *work of adhesion*,²²

$$W_{\text{ad}} = 2\gamma_s - \gamma_{gb}. \quad (1)$$

Here, γ_{gb} and γ_s are the energies per unit area of the

grain boundary and surface whose impurity concentrations are such as to be in equilibrium with the bulk. Equation (1) is known as the Young–Dupré equation²³ when used to analyse the equilibrium contact angle at a droplet on a surface. It is relevant in fracture only if the impurity diffuses very rapidly in the bulk, for example in instances of hydrogen embrittlement. The second case is applicable here, namely that the growth of the crack is so rapid that the impurity remaining at the surfaces has no time to come into equilibrium with the underlying bulk. Indeed at best some surface diffusion may occur as the crack is opening and one may suppose a *local equilibrium*²¹ is achieved in the surface layer of host and impurity atoms.⁶⁴ In that case one identifies $\mathcal{G}_{\text{cleav}}$ with the reversible *work of separation*²² under the constraint that bulk diffusion is suppressed. As now the number of particles, and not their chemical potentials, are fixed during the separation we obtain

$$\mathcal{G}_{\text{cleav}} = W_{\text{sep}}(\Gamma_{gb}) = \frac{1}{A} \{2G_s(\frac{1}{2}\Gamma_{gb}) - G_{gb}(\Gamma_{gb})\}, \quad (2)$$

where A is the surface area, G is the excess Gibbs free energy of a representative piece of material containing either the grain boundary (before decohesion) or the surface (after decohesion), Γ_{gb} is the impurity excess at the grain boundary before cleavage, and we assume that the impurity is evenly distributed between the two newly created surfaces. The excess in Eq. (2) is taken with respect to the adjoining bulk phases.

To express equation (2) in terms of surface and grain boundary energies one can follow the analysis of Hirth and Rice.²¹ Under the condition that the bulk impurity concentration is dilute we may write

$$W_{\text{sep}}(\Gamma_{gb}) = 2\gamma_s(\frac{1}{2}\Gamma_{gb}) - \gamma_{gb} + (\mu'_i - \mu_i)\Gamma_{gb}. \quad (3)$$

This may be useful in revealing two differences between the “slow” and “fast” limiting cases. In finding equation (3) it is necessary to regard the surface atomic layer as a thermodynamic system, uncoupled from the underlying bulk. The impurity atoms have a chemical potential μ'_i , different from their chemical potential μ_i in the bulk and at the grain boundary prior to fracture. One can then interpret $\gamma_s(\frac{1}{2}\Gamma_{gb})$ as the surface energy of a crystal whose bulk composition is such that its equilibrium surface excess is $\frac{1}{2}\Gamma_{gb}$. Secondly, the final term in equation (3) may be interpreted as the energy released to the impurity atoms as a result of the change in chemical potential on finding themselves out of equilibrium with the underlying bulk. This illustrates the point that one would always expect the work of adhesion to be smaller than the work of separation.

Both of the limiting cases embodied in equations (1) and (2), may alternatively be formulated in terms of the work of adhesion or separation of the equivalent grain boundary in pure material \mathbf{A} , say, $W_{\text{sep}}(\mathbf{A})$, plus terms accounting for the presence of impurity.^{5,6} In the case of “fast” fracture, if one neglects a small contribution to

W_{sep} associated with the change of configurational entropy when a grain boundary with impurity splits into surfaces, equation (2) becomes:⁶

$$\mathcal{G}_{\text{cleav}} = W_{\text{sep}}(\mathbf{B}) = W_{\text{sep}}(\mathbf{A}) - G_{\text{seg}}(\mathbf{B}_s) + G_{\text{seg}}(\mathbf{B}), \quad (4)$$

where \mathbf{B} denotes material with segregant, as in figure (1), and $G_{\text{seg}}(\mathbf{B}_s)$ and $G_{\text{seg}}(\mathbf{B})$ are the segregation free energies per unit area of surface and grain boundary respectively. Equation (4) may be interpreted to imply that an impurity which segregates more readily to a free surface than to a grain boundary will cause a reduction in work of separation, or conversely will lead to grain boundary cohesion enhancement.¹⁸ It is worth repeating that a reduction in work of separation does not necessarily imply *embrittlement* which in the simplified picture advocated here requires that $\mathcal{G}_{\text{cleav}} < \mathcal{G}_{\text{disl}}$.

In our *ab initio* supercell calculations the effect of temperature is neglected hence we approximate the Gibbs free energies G_{gb} and G_s in (2) with total energies E_{gb} and E_s of the supercells containing the grain boundary and the surface, respectively. Correspondingly, the segregation free energies in (4) are estimated as the energy required to remove all the impurity from the interface and distribute it in the bulk.

The assumption that impurity atoms distribute evenly between the surfaces in equation (2) may be removed in a straightforward way. Modification to any arbitrary distribution is allowed as long as the surface excesses sum up to that at the grain boundary. For example, if one of the surfaces stays bare, $2G_s(\frac{1}{2}\Gamma_{gb})$ in equation (2) must be replaced with $G_s(\Gamma_{gb}) + G_s(0)$. In principle, one should choose the distribution that minimises the sum of the “surface” Gibbs free energies G_s and therefore the work of separation (2). In our study, we consider two limiting cases having either equal distribution, or all impurities residing on one of the two surfaces. The difference is generally rather modest; experiment usually shows an even distribution of Bi between the surfaces.²⁴

II. STRUCTURAL AND CHEMICAL EMBRITTEMENT

In this section we define concepts of “structural embrittlement” and “chemical embrittlement” precisely. While there is no unique definition that can unambiguously separate structural from chemical effects, we seek a definition that is practical and could be used to rationalise results for many different systems. For this reason a general definition should be unambiguous and independent of the components, including both interstitial and substitutional impurities. For future applications we formulate such a general definition, although the calculations described in this paper are for substitutional impurities only. Furthermore, some modification to the following discussion will need to be made to describe the “slow” fracture of equation (1).

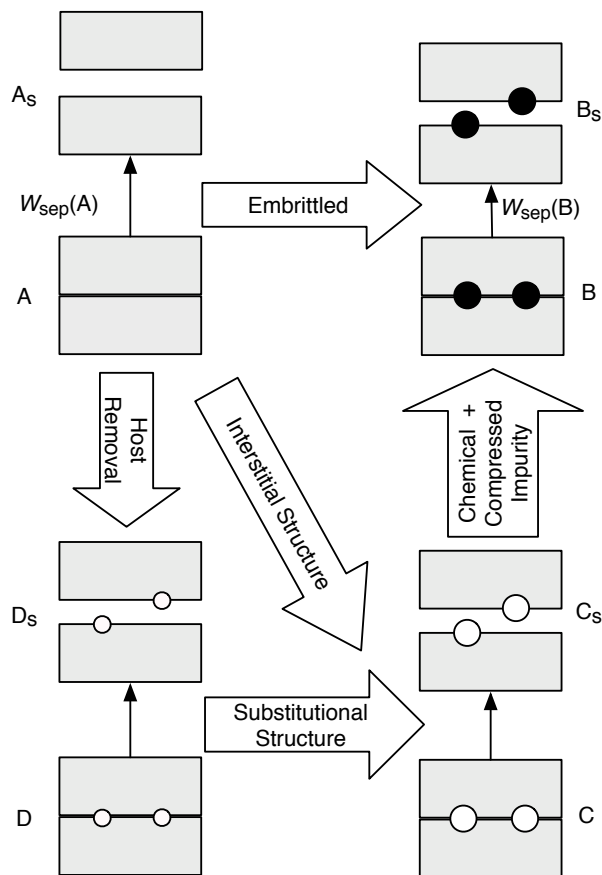


FIG. 1: General scheme for discussion of embrittlement mechanisms due to boundary weakening by impurity segregation. **A** and **B** denote the fully relaxed equilibrium unsegregated and segregated grain boundaries, respectively. Boundary **C** is created by substituting impurity atoms in **B** (black spheres) with vacancies (white spheres) without further relaxation, and **D** is created from **A** in the same way. **A_s**–**D_s** denote the free surfaces into which grain boundaries **A**–**D** cleave. Path **A**→**D**→**C**→**B** refers to substitutional impurities, whereas path **A**→**C**→**B** applies to interstitial impurities.

A. Intermediate configurations

In order to proceed we need to define a number of hypothetical reference systems (see figure 1), which we denote **A**, **B**, **C** and **D**. Each system is in the form of a grain boundary of unit area and separated surfaces, the latter being distinguished from the grain boundary by the suffix **s**.

These systems refer to a given host and impurity combination, a given grain boundary and a given distribution of impurity atoms at the boundary. A system comprising separated surfaces should have exactly the same total numbers of atoms of each species as the corresponding grain boundary, so that bulk quantities will cancel out of all the relevant energy differences, as described by works of separation. To avoid a complicated

treatment of ensembles that would be required to deal with more concentrated solutions, we assume that on the length scale of a supercell⁶⁵ the bulk can be treated as pure host. The systems are defined as follows:

A: The relaxed grain boundary of the pure host.

A_s: The relaxed, separated surfaces corresponding to **A**.
B: The relaxed grain boundary of the host with segregated impurity atoms.

B_s: The relaxed, separated surfaces corresponding to **B**.

C: The same atomic structure as **B**, with impurity atoms removed from the impurity sites defined in **B** but no further relaxation. We refer to the imprint of these absent impurities as “ghosts” since they define forces that maintain the host atoms in a distorted structure, but make no other direct contribution to the energy. For substitutional impurities a ghost is a more or less strained vacancy. For interstitial impurities a ghost is a centre of strain in the host lattice without missing atoms.

C_s: The same atomic structure as **B_s**, with impurity atoms removed from the impurity sites defined in **B_s** but no further relaxation.

D: This system is only relevant for substitutional impurities such as those discussed in the rest of this paper. It is the same structure as **A**, with host atoms removed from the impurity sites defined in **B** but no further relaxation.

D_s: The same atomic structure as **A_s**, with host atoms removed from the impurity sites defined in **B_s** but no further relaxation.

Some points of clarification may help to visualise these systems. Note first that **A**, **A_s**, **B** and **B_s** label fully relaxed structures, whereas **C**, **C_s**, **D** and **D_s** label notional structures we set up in the computer using the atomic positions found for the relaxed systems. The works of separation for each system are defined as the differences in total energy, for example for system **A**:

$$W_{\text{sep}}(\mathbf{A}) = E(\mathbf{A}_s) - E(\mathbf{A}). \quad (5)$$

Although we would prefer E to mean the Gibbs free energy, for simplicity of calculation we use as a surrogate the total energy at 0 K (see section I). A more exact calculation could be made in principle, to include phonon free energies in the harmonic approximation.

If the impurity is detrimental to cohesion, the work of separation of our embrittled boundary, **B**, is less than the work of separation of the clean boundary, $W_{\text{sep}}(\mathbf{A}) - W_{\text{sep}}(\mathbf{B}) > 0$. As summarised in section I, this picture of grain boundary weakening is equivalent to the statement that surface segregation is energetically preferred to grain boundary segregation, that is, from equation (4),

$$W_{\text{sep}}(\mathbf{A}) - W_{\text{sep}}(\mathbf{B}) = G_{\text{seg}}(\mathbf{B}_s) - G_{\text{seg}}(\mathbf{B}) > 0. \quad (6)$$

These formulations of the difference show how the bulk energies, including the energy contribution of dissolved

impurities, cancel out. We are now in a position to discuss what we mean by a “size effect” or “structural effect” as opposed to a “chemical effect”.

B. Size effects and chemical effects

Leaving aside for the moment chemical effects, we might regard a misfitting impurity in the bulk as storing energy mechanically, like a compressed or stretched spring. The stored energy is fully released when the impurity segregates to a surface, but only partially released when the impurity segregates to a grain boundary. This would be a simple mechanical picture of the origin of the embrittlement. However, it is unsatisfactory without specifying what happens to the stored energy. Consider the case of an oversized and therefore substitutional impurity. If it found a sufficiently loose site at the grain boundary, it could eliminate the strain energy and lower the grain boundary energy by segregating there. In this case there would be no further reduction in stored energy on cleavage. The net effect would therefore be an *increase* in W_{sep} . While the stored energy in an oversized, compressed impurity is likely to be a driving force for getting it to a boundary, what matters for embrittlement is how much of this energy is *stored* in the boundary, to be released on cleavage. It is stored in three ways: (i) as broken host–host bonds, because the impurity substitutes for the host; (ii) as stretched host–host bonds; and (iii) in the compressed or expanded impurity atoms themselves.

If the impurity is interstitial, the first of these is irrelevant, since we suppose that no host–host bonds in the boundary are broken by the presence of the impurity. The first two contributions are illustrated in figure 1 by the paths labelled “Host Removal (HR) \rightarrow Substitutional Structure (SS)” and “Interstitial Structure (IS)” respectively. System **D** was introduced solely for the purpose of quantifying the magnitude of the substitutional effect, by removing the effects of bond-stretching. Accordingly we define the following contributions to the path from **A** to **C** for substitutional structures:

$$\text{HR} = W_{\text{sep}}(\mathbf{D}) - W_{\text{sep}}(\mathbf{A}) \quad (7)$$

$$\text{SS} = W_{\text{sep}}(\mathbf{C}) - W_{\text{sep}}(\mathbf{D}), \quad (8)$$

and for interstitial impurities

$$\text{IS} = W_{\text{sep}}(\mathbf{C}) - W_{\text{sep}}(\mathbf{A}).$$

The final step around the diagram in figure 1, labelled “Chemical + Compressed Impurity (CC)” takes the system from **C** to **B**:

$$\text{CC} = W_{\text{sep}}(\mathbf{B}) - W_{\text{sep}}(\mathbf{C}). \quad (9)$$

This is where the chemistry of the impurity comes into play. Notice that in this step the host atoms are in the

same positions with and without the impurity, so no further energy change is associated with the energy stored in the host lattice. However, if we are thinking mechanically, there may still be some energy released by volume relaxation of the impurities in going from the grain boundaries to the surfaces. We might expect this to be more significant when the grain boundary concentration is low, in which case there are still some host–host bonds holding the impurities in a state of compression, compared to the case of say a monolayer of segregation, in which the local volumes of the impurities are much more relaxed. However, it does not seem possible or useful in the step from **C** to **B** to try to separate this from the chemical contribution, which contains the energy of the impurity–host bonds that are broken. Note that our IS and CC mechanisms are respectively the “mechanical” and “chemical” contributions identified in refs. [25,26] in the context of interstitial impurities.

What would be the likely effect of the contributions just considered on the work of separation? The HR mechanism should *decrease* W_{sep} since removal of a host atom cuts more bonds at a grain boundary than at a surface. Conversely, the CC step is expected to *increase* W_{sep} , although the necessity to squeeze an oversized impurity while inserting it into a grain boundary acts so as to reduce the effect. The reduction should be most pronounced for tight grain boundary sites or large and soft impurity species. (By “large” and “soft” we imply a measure such as found in table VI, below.) Finally, the SS step must *decrease* W_{sep} for an oversized impurity, as the only way for such an impurity to accommodate itself at the grain boundary is to push the grains apart, whereas at a free surface it may protrude into the vacuum without significantly distorting its surrounding host atoms.

The interstitial impurity case reduces to the competition between only two mechanisms (IS and CC); the result can be of either sign.^{12,25,26} Interestingly, the IS mechanism tends to *strengthen* the boundary for small impurities (H, B, C, N, and O) as they distort free surfaces more than grain boundaries by occupying subsurface sites, whereas the effect of the CC mechanism can be either positive or negative depending on the nature of chemical bonds formed between impurities and host atoms.^{25,26} Indeed, in ref [26] it is found that B and C enhance the cohesion of grain boundaries in Mo, while N and O reduce the work of separation; the contribution of the CC mechanism also acts to lower W_{sep} if the impurity is C, O or N, while only for B does the CC mechanism lead to cohesion enhancement at their grain boundary in Mo.

We show in what follows that one can carry the system around the *gedanken* path in figure 1 explicitly by calculating the quantities defined by equations (7)–(9) and hence identify the magnitudes of the “size” and “chemical” contributions to grain boundary decohesion.

III. CALCULATION DETAILS

We have calculated the atomic and electronic structure of the $\Sigma 5$ grain boundary in copper from first principles using the full potential LMTO method as implemented in the NFP code.²⁷ In this code, wavefunctions and charge density are expanded in smooth Hankel functions having an energy $-\kappa^2$ and a smoothing radius r_{sm} defined such that beyond r_{sm} smooth and singular Hankel functions are not appreciably different. For each atom type we employ two such envelope functions for each angular momentum quantum number up to some ℓ_{max} . These are augmented inside atomic spheres with numerical solutions of the radial Schrödinger equation; all relativistic effects except spin orbit coupling are included, the core is permitted to relax to self consistency but is treated as spherical. In the *interstitial region* outside the atomic spheres, the Poisson equation is solved analytically in the smooth Hankel basis and the exchange–correlation energy and potential are obtained through a real space grid representation. We use the local density approximation (LDA) in the parameterisation of von Barth and Hedin, modified by Moruzzi *et al.*^{28,29} Basis function parameters and atomic sphere radii used in our study, are shown in table I. For Bi we additionally included a localised orbital to allow the Bi $5d$ semi core to be treated as a valence state in addition to the $6d$ valence state.

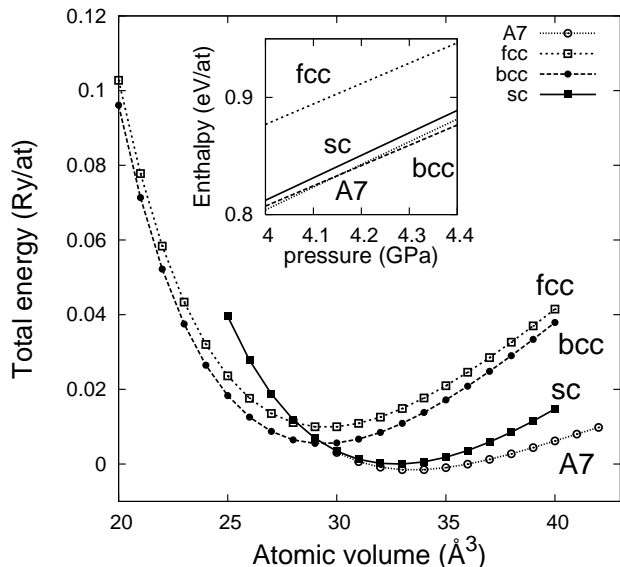


FIG. 2: Energy–volume curves for bulk Bi. A fragment of the respective enthalpy–pressure plot near the bcc–A7 crossover is shown in the inset. The energy and enthalpy are measured relative to those of Bi(A7) at zero pressure.

Some bulk properties of Cu and Bi obtained in our LDA calculations are listed in table II where they are compared with experiment and other LDA calculations. Figure 2 shows calculated energy–volume curves for bulk Bi. In agreement with experiment, the rhombohedral

A7 structure has the lowest energy. With pressure increasing, the A7 curve gradually merges into the simple cubic curve, the rhombohedral angle steadily increasing towards 60° and the internal coordinate u tending to its symmetrical value of 0.25. However, at a pressure of 4.2 GPa the A7 curve is intersected by the bcc curve. In experiment, the bcc structure becomes stable above 7.7 GPa, although there are two more phases, Bi–II and Bi–III, which appear between A7 and bcc.³¹ These are rather complex and were not considered in our study.

The grain boundary was represented in our calculations with a periodic supercell containing two identical grain boundaries separated by nineteen (310) layers (38 atoms). The equilibrium width of the grain boundary was determined by stretching the supercell along the interface normal and finding the minimum of the total energy of the resulting relaxed supercell as a function of the stretch. The lateral dimensions of the supercell were fixed by the theoretical equilibrium lattice parameter of the bulk fcc copper (table II). Atomic positions were fully relaxed in each of the supercells considered until the forces dropped below 1 mRy/Bohr. No finite temperature effects were taken into account. As the equilibrium structure of the $\Sigma 5(310)[001]$ grain boundary in Cu is well known from previous theoretical⁴⁰ and experimental¹⁵ studies, in our calculations we have not attempted to further optimise the atomic structure of the grain boundary by shifting the adjacent grains laterally. To minimise systematic errors in calculating the work of separation, the energy of free surfaces was obtained using the same supercell, in which about half of the copper layers were replaced with the vacuum so that no grain boundary remains. For the same reason, we filled the whole supercell with atoms (so called “space filling slab” geometry) for the reference bulk calculations. For calculating grain boundary and surface excess free energies, equation (2), at different coverages and hence different stoichiometries of the slabs we employ standard formulas^{41,42} taking the chemical potentials of the components from bulk calculations.

Calculations were done for impurity atoms (Bi, Na, or Ag) replacing 0, 1 (“loose” site, see figure 3), and 2 atoms at the grain boundary plane, which we refer to as 0, 0.5 ML, and 1 ML coverage, respectively. In addition, we considered the grain boundary with Bi at 0.25 ML coverage by doubling the supercell along the [001] tilt axis and replacing every *other* Cu atom in the “loose” position with Bi. In all supercell calculations, a $16 \times 10 \times 2$ Monkhorst–Pack mesh of k -points was employed with a Methfessel–Paxton broadening factor⁴³ of 5 mRy. To represent the smooth interstitial electronic density,²⁷ a $24 \times 38 \times 152$ real space mesh was employed. In practical terms, a significant speed up of the calculations was achieved by performing the relaxation first with a somewhat reduced set of parameters ($8 \times 4 \times 2$ k -point mesh and a $18 \times 25 \times 96$ real space mesh) employing the criterion that forces were stabilised within 1–2 mRy/Bohr, and then further optimising the positions using the finer

TABLE I: Double basis set parameters used in the present study: atomic radius, r_a , smoothing radii r_{sm} , and energetic parameters $-\kappa^2$ for each angular momentum ℓ . Radii r_a are chosen so that atomic spheres would not overlap by more than few percent in all configurations considered.

Species	r_a , Bohr	r_{sm}/r_a				$-\kappa^2$, Ry			
		$\ell = 0$	$\ell = 1$	$\ell = 2$	$\ell = 3$	$\ell = 0$	$\ell = 1$	$\ell = 2$	$\ell = 3$
Cu	2.238	0.761	0.667	0.442		-0.600	-0.400	-0.400	
		0.761	0.831	0.417		-1.000	-1.000	-1.000	
Bi	2.450	0.801	0.756	0.486	0.800	-0.911	-0.374	-0.400	-0.400
		0.801	0.756	0.486	0.800	-3.000		-3.000	-1.000
Na	2.450	0.569	0.582	0.469		-1.636	-0.400	-0.400	
		0.569	0.582	0.469		-2.000	-2.000	-2.000	
Ag	2.450	0.528	0.551	0.408		-1.031	-0.400	-0.555	
		0.528	0.551	0.408		-3.000	-3.000	-3.000	

TABLE II: Bulk properties of Cu and Bi: lattice constant, a_0 , rhombohedral angle, α , and internal coordinate, u , of the equilibrium crystal structure (fcc for Cu, and A7 for Bi), structural energy differences, ΔE_β with respect to that structure, bulk modulus, B , and elastic constants, $C' = (c_{11} - c_{12})/2$ and c_{44} , obtained in the present study, other scalar relativistic (unless indicated otherwise) LDA calculations, and experiment.

	Cu			Bi		
	our LDA	other LDA	Exp.	our LDA	other LDA	Exp.
a_0 , Å	3.5270	3.53 ^a , 3.52 ^b , 3.58 ^c , 3.52 ^d	3.6146 ³⁰	4.6211	4.62 ^a , 4.528 ^e	4.7460 ³¹
α				58.25 ^o	58.23 ^{o a} , 58.93 ^{o e}	57.23 ^{o 31}
u				0.2370	0.238 ^a , 0.238 ^e	0.2341 ³¹
ΔE_{fcc} , mRy	0	0	0	11.4		
ΔE_{bcc} , mRy	2.7	2.9 ^a , 3.2 ^f		7.0		
ΔE_{sc} , mRy	39.4	40.0 ^f		1.5		
B , GPa	185.9	190 ^a , 192 ^b , 153 ^c , 190 ^d	137 ³²	43.4	46 ^a , 51 ^a	38.2 ³¹
C' , GPa	31.2	35 ^a , 27.2 ^c , 25 ^d	23.5 ³³			
c_{44} , GPa	98.9	99 ^a , 86 ^c , 80 ^d	75 ³³			

^a Ultra soft pseudopotentials, Refs. [13,34].

^b LAPW, ref. [35].

^c Full potential LMTO, non-relativistic, ref. [36].

^d Full potential LAPW, ref. [37].

^e Norm conserving pseudopotentials, ref. [38].

^f LAPW, ref. [39].

set of meshes. A typical difference between the work of separation and grain boundary expansion obtained with either set of parameters, 0.05 J/m² and 2 pm, respectively, can be taken as a “pessimistic” estimation of the convergence of our calculations with respect to the number of k -points and to the size of the real space mesh.

Fully relaxed calculations of the impurity atoms in Cu bulk were done using 32 atom cubic cells with an 8×8×8 k -point mesh and a 48×48×48 real space mesh.

IV. PURE COPPER $\Sigma 5$ GRAIN BOUNDARY

The atomic structure of the relaxed $\Sigma 5(310)[001]$ symmetric tilt grain boundary in pure Cu obtained in the

present study, is shown in figure 3a, as viewed along the [001] direction. It contains two alternating (001) planes separated by half the lattice constant, a_0 , shown with larger and smaller circles. It can be imagined as a mirror related twin boundary structure in which one of the two (310) boundary planes in either grain bordering the mirror plane is removed, while the other one collapses into the grain boundary plane. The same structure can be obtained by arranging a suitable lateral shift for the upper half of the original twin with subsequent relaxation.⁴⁰ One ends up with two non-equivalent atoms at the grain boundary plane, one of which being in the “loose” environment and the other being in the “tight” environment. The former provides a natural substitutional site for an oversized impurity. A recent experimental STEM

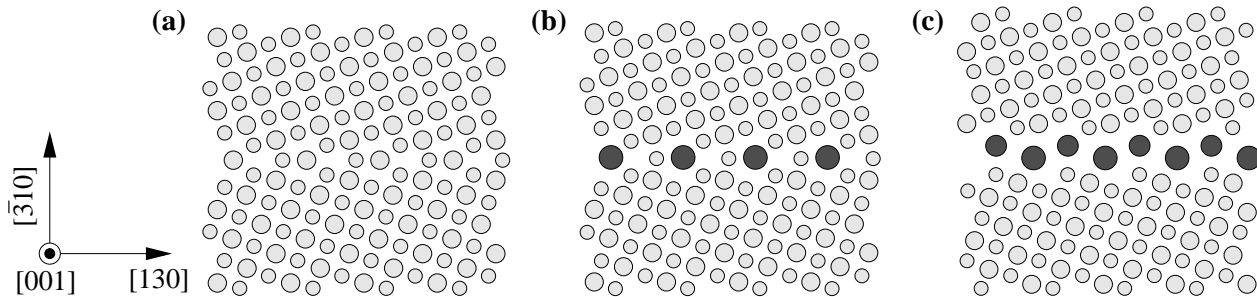


FIG. 3: Relaxed atomic structure of the Cu $\Sigma 5(310)[001]$ grain boundary: (a) Pure copper; (b) with 0.5 ML of Bi; and (c) with 1 ML of Bi at the grain boundary plane. Notice that in the pure grain boundary (a) there are two inequivalent atomic positions in the boundary plane. We refer to these as “loose” (the larger circle) and “tight” (the smaller circle) to illustrate the average distance of the nearest neighbours. Naturally we expect a larger atom preferentially to select the loose site to occupy.

TABLE III: The energy of the (310) surface, γ_s , and of the $\Sigma 5(310)[001]$ grain boundary, γ_{gb} , the grain boundary width, w (grain boundary excess volume per unit area), and the work of separation, W_{sep} , in pure Cu. Experimental data and the results of other calculations are given in parentheses. For comparison, the results for the $\Sigma 19a(331)[\bar{1}10]$ grain boundary and (331) surface¹³ are also shown.

Pure Cu	$\Sigma 5$	$\Sigma 19a^d$
w , Å	0.28	0.22
γ_s , J/m ²	2.21 (1.77 ^a)	2.07
γ_{gb} , J/m ²	1.07 (0.980 ^b , 0.888 ^c)	1.04
W_{sep} , J/m ²	3.35	3.10

^a Exp. polycryst., ref. [44].

^b Finnis-Sinclair many-body potentials, ref. [45].

^c EAM, ref. [40]. ^d Ultra soft pseudopotentials, ref. [13].

image of the grain boundary¹⁵ is very similar to that depicted in figure 3a. The calculated grain boundary energy (table III) is in good agreement with semi empirical data. In addition, the $\Sigma 5$ results listed in the table are close to those of *ab initio* calculations obtained for the $\Sigma 19a(331)[\bar{1}10]$ grain boundary in pure Cu.¹³ The works of separation of both grain boundaries are sufficiently large to ensure that the boundaries are ductile according to the criterion $W_{sep} > \mathcal{G}_{disl} \simeq 1-2$ J/m² as they should be.

V. COPPER $\Sigma 5$ GRAIN BOUNDARY WITH BISMUTH

The relaxed atomic positions of the $\Sigma 5$ grain boundary with 0.5 ML of Bi are shown in figure 3b; those for the 0.25 ML of Bi are very similar except that the grain boundary expansion is about half as large (see table IV).

We define the grain boundary expansion as the difference per grain boundary between the lengths of supercell with and without impurity atoms, noting that supercells contain the same number of atoms since our impurities

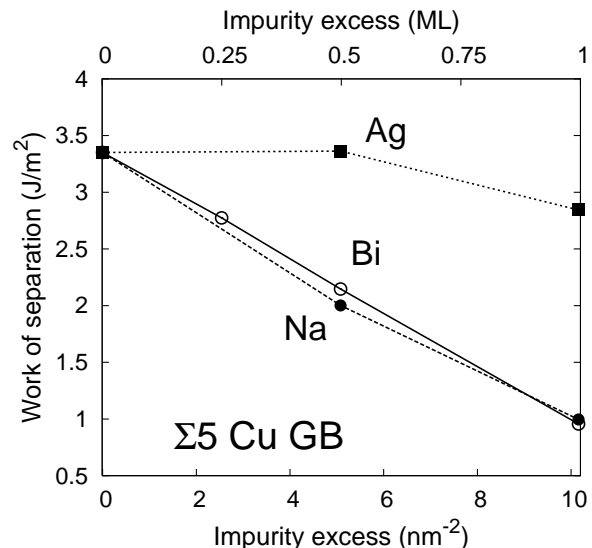


FIG. 4: Dependence of the work of separation on the impurity excess at the $\Sigma 5(310)[001]$ Cu grain boundary: Bi (open circles), Na (filled circles), and Ag (filled squares).

are *substitutional*. In view of the large discrepancy in the grain boundary expansion of 50.9 pm for the 0.5 ML Bi segregated grain boundary obtained in the present study compared with the calculation of Duscher *et al.*,¹⁵ namely 7–10 pm, using the ultra soft pseudopotentials (USPP) within the VASP code,⁴⁶ we have additionally computed the expansion of one of the $\Sigma 19a$ boundaries with 1 ML of Bi, for which we already knew the USPP result obtained with the VASP code.³⁴ As the NFP and VASP expansions were found to agree within 6% (102 pm and 108 pm, respectively) we can safely conclude that the grain boundary expansions listed in table IV are the correct results within the local density approximation.

The work of separation and the grain boundary expansion in table IV are also plotted in figs. 4 and 5 against the Bi excess at the boundary. Up to 0.5 ML of Bi, both quantities comfortably fall on a straight line, meaning

TABLE IV: Grain boundary expansion and work of separation of the $\Sigma 5(310)[001]$ Cu grain boundary with impurities. Grain boundary coverage of 0.5 ML and surface coverage of 1 ML correspond to an areal density of 5.08 impurity atoms per nm^2 .

	Cu		Bi		Ag		Na	
Impurity excess, ML	–	0.25	0.5	1	0.5	1	0.5	1
GB expansion δ , pm	0	25.7	50.9	159.2	13.0	44.5	31.1	154.6
Segregation energy, eV:								
to the (310) surface	0		3.11	3.01	0.77	0.77	3.00	2.70
to the grain boundary	0	1.69	1.63	1.54	0.79	0.46	1.34	1.26
W_{sep} , J/m^2 :								
into 0.5 + 0.5 surfaces	3.35		2.15	0.96	3.37	2.84	2.00	1.00
into 1 + 0 surfaces	3.35	2.77	2.23	1.85	3.36		2.24	

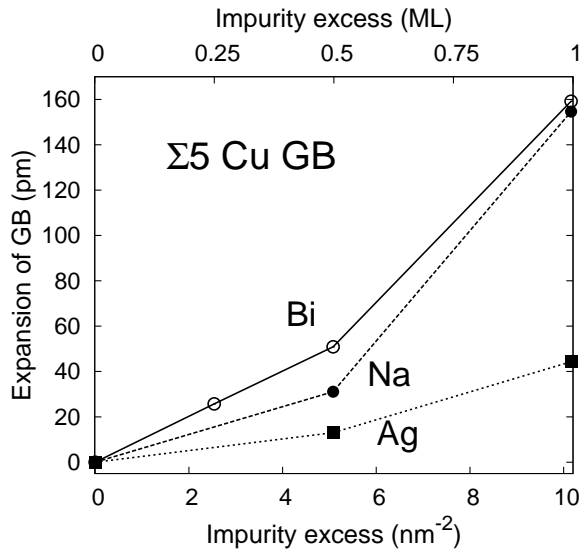


FIG. 5: Same as figure 4 but for the grain boundary expansion.

that while Bi atoms fill the “loose” sites their effect is additive.

Although the work of separation decreases as Bi progressively substitutes Cu at the “loose” sites of the grain boundary, even at 0.5 ML it remains larger than G_{disl} , which implies that up to that coverage, *the boundary is ductile*. This will have been the situation in the work of Duscher *et al.*¹⁵ From experiment it is known that the $\Sigma 5$ grain boundary is *severely* embrittled by Bi.^{16,47} We therefore proceeded to add more Bi at the grain boundary by replacing Cu both at the “loose” and “tight” sites (1 ML). In this calculation we did not fully optimise the grain boundary structure with respect to rigid lateral shifts of the grains, however we removed the mirror symmetry constraint so that the grains could move during the atomic relaxation if they wished. As can be seen in figure 3c, the relaxed structure of the grain boundary does show a significant lateral displacement of the grains; in addition the Bi layer substantially buckles giving rise to large increase of the grain boundary width. The buckling

of the grain boundary plane is due to large Bi atoms being too close to each other, perhaps the structure shown in figure 3c can be considered as a precursor of the grain boundary faceting which is often detected at Cu grain boundaries with Bi.^{48,49,50} Specifically in the $\Sigma 5$ grain boundary, some “roughening” has been reported.⁴⁵

The work of separation of the Cu grain boundary with 1 ML of Bi drops below $1 \text{ J}/\text{m}^2$ which we take as an indication that the threshold concentration of the impurity required to embrittle the grain boundary, has been reached. Note in passing that the way in which impurity atoms distribute themselves between the surfaces after cleavage turns out to be of little importance; the case of equal distribution (denoted as “0.5 + 0.5” in table IV), is marginally lower in energy than the case when all Bi atoms reside on one of the surfaces (“1 + 0” in table IV). The exception is the “1 + 0” separation of the 1 ML grain boundary demonstrating a sizeable increase of W_{sep} .

The segregation energies of Bi to the grain boundary depend weakly on Bi concentration there (which is just another way to say that the $W_{\text{sep}}(T)$ dependence is linear) and are significantly smaller than the segregation energies to the free (310) surface, as is expected for an embrittling impurity (see Sec. I). Our grain boundary segregation energies are comparable to those obtained for the $\Sigma 19a$ boundary,¹³ namely 1.32 eV for 0.5 ML and 1.58 eV for 1 ML per impurity atom. The experimentally reported Gibbs segregation free energy to the $\Sigma 5$ boundary at $T = 700^\circ\text{C}$ is $G_{\text{seg}} = 0.92 \pm 0.11 \text{ eV}$ —markedly smaller than our theoretical values. This was, however, the largest segregation energy among the all grain boundaries studied in ref. [45]. The difference may well be due to the effect of vibrational entropy. McLean⁵¹ argued that the segregation to grain boundaries of solute atoms sufficiently larger or smaller than the host atoms, results in the atomic packing becoming denser at the grain boundary, hence the vibrational entropy of the grain boundary region may decrease. Decrease of the vibrational entropy has been recently predicted for Ag segregating to the $\Sigma 5$ grain boundary plane in Cu.⁵²

TABLE V: Enthalpy of solution, H_s , and the relative dilation volume, Ω_d/Ω_0 , per impurity atom of Bi, Ag, and Na in bulk fcc Cu. Ω_d is defined as the difference of the equilibrium volumes of the cell with and without impurity at constant number of atoms, and Ω_0 is the equilibrium atomic volume of pure Cu. The last column gives the formation enthalpy (in eV) and formation volume (in units of Ω_0) of a vacancy in bulk Cu.

Impurity:	Bi	Ag	Na	Vac
H_s , eV: this work	1.66	0.50	1.73	1.27
other calc.	1.7 ^a	0.83 ^b	1.33 ^{b,f} , 1.29 ^g	
exp.		0.39 ^c	1.28 ^h	
Ω_d/Ω_0 : this work	1.40	0.54	0.67	0.64
other calc.	1.3 ^a	0.64 ^b , 0.52 ^d		0.70 ^{b,d}
exp.		0.45 ^e , 0.58 ^e		0.75 ^h

^a Ultra soft pseudopotentials, Refs. [13,34].

^b LSGF, unrelaxed, ref. [54].

^c Exp., ref. [55].

^d FP-KKR, ref. [56].

^e Exp., ref. [57]. ^f FP-LMTO, ref. [58].

^g FP-KKR, ref. [59].

^h Exp., ref. [60].

VI. COPPER $\Sigma 5$ GRAIN BOUNDARY WITH SODIUM AND SILVER

If Bi embrittlement is a purely structural effect which has nothing to do with Bi’s chemical identity, then the same behaviour is expected from other elements which, say, are of about the same size as Bi and are not engaged in any strong chemical bonding with the host atoms (see section II for a more detailed discussion of structural embrittlement). In ref. [13] it was shown that Pb behaves very similarly to Bi. One can argue, however, that since Bi and Pb are neighbours in the Periodic Table, such similarity is indeed expected. We therefore decided to pick an element as different to Bi as possible, from which only structural embrittlement is expected. For this reason, we chose the alkali metal Na. Like Bi it does not form any stable compounds with Cu and has vanishingly small solubility.⁵³ Indeed, the calculated enthalpy of solution of Na in fcc Cu is as large as that of Bi (table V). In addition, the lattice constants of Na and Bi, both calculated in a hypothetical fcc structure, are close to each other and much larger than the lattice constant of Cu (table VI). Na, however, is a much softer species than Bi as is exemplified by its smaller bulk modulus (table VI) and solute dilation volume (table V).

The other element that we have chosen for comparison is Ag for it is known that silver *does not* embrittle Cu. The lattice constant of fcc Ag is nevertheless larger than that of Cu, and the heat of solution of Ag in Cu is positive, although these are not as extreme as for either Bi or Na. The experimental Ag–Cu phase diagram shows noticeable solubility of Ag in Cu (up to 5%), but without the formation of stable compounds.⁵³

TABLE VI: Lattice constant, a_0 , and bulk modulus, B , of the impurity species calculated in bulk fcc structure. These data may be used as a measure of the relative “size” and “softness” of atoms.

Impurity:	Cu	Bi	Ag	Na
a_0 , Å	3.5270	4.9048	4.0218	4.9779
B , GPa	185.9	64.7	135.3	15.8

TABLE VII: Works of separation W_{sep} (in J/m²) corresponding to configurations **A–D** in figure 1 for impurity coverages of 0.5 and 1 ML. Configuration **A** (pure boundary) of course does not depend on impurity coverage.

Impurity	0.5 ML				1 ML		
	A	B	C	D	B	C	D
Bi	3.35	2.15	1.81	2.20	0.96	0.13	1.38
Na	3.35	2.00	1.97	2.20	1.00	0.14	1.38
Ag	3.35	3.37	2.17	2.20	2.84	1.01	1.38

The grain boundary calculations with Na and Ag were done in the same way as for Bi. The expansion of the grain boundary with 0.5 ML of Na is smaller compared to Bi, however the grain boundary with 1.0 ML of Na expands by almost the same amount as with Bi (see table IV and figure 5). This can be understood assuming that Na is a softer species than Bi, but of slightly larger size (see table VI) and taking into account that the fall off of the mutual attraction between Cu grains with distance is faster than linear. In all other respects Bi and Na behave strikingly similarly (see table IV and figure 4). In particular, we observe that Na renders the grain boundary brittle at 1 ML coverage. This is our prediction, as no experimental studies of Na at Cu grain boundaries seem to exist. However, there are indications that Na can embrittle Cu in the context of liquid metal embrittlement.⁶¹

The similarity between Bi and Na provides evidence that charge transfer effects are of negligible importance. If for example the major cause of the embrittlement were weakening of Cu–Cu bonds due to transfer of electrons *from* Bi *to* Cu as proposed in ref. [15], then a free electron metal such as Na would have led to even stronger embrittlement, say, at 1 ML coverage where the grain boundary expansion for Bi and Na is the same. This is not observed in our calculations.

Silver, on the other hand, does not bring about any significant decrease of W_{sep} even at 1 ML (table IV and figure 4). In fact, at 0.5 ML coverage it even slightly strengthens the boundary, despite a small expansion of the latter. Such a peculiar situation arises because Ag atoms turn out to be of just the right size to replace Cu at the “loose” sites. The resulting denser packing at the grain boundary thus compensates the replacement of Cu–Cu bonds with slightly weaker Cu–Ag bonds. Interestingly the energy of Ag segregation to the grain boundary decreases in going from 0.5 ML to 1 ML: this simply

TABLE VIII: Impurity segregation energies (in eV per impurity atom) related to W_{sep} in table VII by virtue of equation (4). The sign convention is such that a positive energy means that the impurity wants to segregate. Note that the impurity in configurations **C** and **D** is actually a vacancy, both in the bulk and at the interface (see section II).

Impurity	0.5 ML						1 ML					
	B		C		D		B		C		D	
	surf	gb	surf	gb	surf	gb	surf	gb	surf	gb	surf	gb
Bi	3.11	1.63	1.18	-0.71	1.20	-0.22	3.01	1.54	1.23	-0.75	1.22	0.02
Na	3.00	1.34	1.24	-0.46	1.20	-0.22	2.70	1.26	1.27	-0.70	1.22	0.02
Ag	0.77	0.79	1.21	-0.25	1.20	-0.22	0.77	0.46	1.25	-0.19	1.22	0.02

TABLE IX: The changes in W_{sep} (in J/m^2) corresponding to Substitutional Structure (SS), Host Removal (HR), and Chemical + Compressed Impurity (CC) mechanisms as defined in figure 1. Negative numbers indicate a decrease in W_{sep} . For Bi and Na, the HR mechanism provides the largest contribution. However, at 1 ML its relative importance diminishes with the SS mechanism contributing nearly half of the overall decrease of W_{sep} . The CC mechanism always acts so as to increase W_{sep} . For Ag, the dominant contributions come from the HR and CC mechanisms which are nearly compensating. (This is an almost trivial result. If we employed Cu as the “impurity” then HR and CC would both be large and would exactly cancel, while SS would be zero.)

Impurity	0.5 ML				1 ML			
	Total	SS	HR	CC	Total	SS	HR	CC
Bi	-1.20	-0.39	-1.15	0.34	-2.39	-1.25	-1.97	0.83
Na	-1.35	-0.23	-1.15	0.03	-2.35	-1.25	-1.97	0.86
Ag	0.02	-0.04	-1.15	1.20	-0.51	-0.37	-1.97	1.83

reflects the attractive nature of the “loose” site to the slightly larger Ag atom.

VII. HOW DOES BISMUTH EMBRITTLE COPPER?

In accordance with the analysis presented in Sec. II, we have created intermediate configurations **C** and **D** defined in Sec. II A which together with fully relaxed pure (**A**) and segregated systems (**B**) form a complete set of data required. The works of separation for each of these configurations corresponding to 0.5 ML and 1 ML coverages are listed in table VII. These works of separation are further split into surface and grain boundary contributions in terms of the segregation energies in table VIII. Finally, table IX shows the changes of W_{sep} invoked by transitions between the configurations **A–D** that give the contributions of the Substitutional Structure (SS), Host Removal (HR), and Chemical + Compressed Impurity (CC) mechanisms, see equations (7)–(9) in Sec. II B.

For the $\Sigma 5$ grain boundary containing 0.5 ML of Bi, which is not yet embrittled, we observe that removal of host atoms from pure boundary sites that will become occupied by Bi (the HR mechanism) strongly dominates

and almost fully accounts for the total decrease of W_{sep} in table IX. The effect of mechanical distortion (the SS mechanism) is modest and is similar in magnitude to the effect of insertion of Bi back into a vacant site—the CC mechanism. This mechanism always acts so as to strengthen the boundary. This is exactly what one would expect from Ag but perhaps not from Bi if one subscribed to the “electronic” point of view. Since the Compressed Impurity contribution can only decrease W_{sep} , yet CC is positive, it is clear that the Chemical mechanism is a large effect tending to increase the work of separation. Even though the grain boundary **C** is pre-stretched, the fact that replacing a vacancy even with Bi increases the intergranular cohesion is yet another demonstration that the *electronic* grain boundary weakening mechanism of embrittlement can be safely ruled out. *The introduction of Bi divorced from any other effect does not weaken the boundary—it strengthens it.*

Increasing Bi coverage to 1.0 ML results in a much larger expansion of the grain boundary. The SS contribution increases substantially giving almost half of the overall decrease of W_{sep} . The HR term still dominates, since twice as many Cu atoms are removed from the grain boundary plane. Correspondingly, the positive CC contribution also increases, but the sum of all three is large enough to render the grain boundary brittle. We therefore conclude that Bi embrittlement of the Cu grain boundary may be attributed to both the Host Removal and Substitutional Structure mechanisms with the relative weight of the latter increasing as the coverage increases.

The effect of Na is strikingly similar to that of Bi (table IX), especially for 1 ML coverage where not only the total effect but even the contributions of each mechanism are almost identical. Hence everything said about Bi can be transferred to Na. At 0.5 ML, the fact that sodium atoms are “softer” but “larger” (see table VI) becomes noticeable with some interesting consequences. The grain boundary expansion and hence the SS contribution is smaller but the total decrease of W_{sep} is larger for Na than for Bi. This is because the CC contribution is almost zero. It would not be correct to conclude that the bonding between Na and Cu is very weak for the effect of CC at 1 ML is as large as for Bi. This is a perfect demonstration of the effect of the Compressed

Impurity mechanism which combines with the Chemical contribution having opposite sign and nearly cancels it out.

Silver does not embrittle Cu grain boundaries, and indeed we observe that the HR and CC contributions strongly dominate but almost cancel each other (but see the caption to table IX). At 0.5 ML the “loose” site is so attractive for a slightly larger Ag atom that it binds there more strongly to other host atoms than even Cu itself does, with negligible grain boundary expansion. At 1 ML silver has to replace Cu at “tight” sites. As a result, HR + CC changes sign and the grain boundary expands. These combine to decrease W_{sep} by very small amount which is insufficient to lead to embrittlement.

VIII. SUMMARY AND CONCLUSIONS

We have investigated *atomic level* mechanisms in the embrittlement of the $\Sigma 5(310)[001]$ grain boundary in Cu by Bi atoms. To this end, we did first principles calculations of the grain boundary with up to 1 ML of impurity atoms: Bi, Na, and Ag. We had two principal aims.

1. Our first was to settle the controversy concerning whether embrittlement is a *structural* or an *electronic* effect. We can reconcile our earlier claim in ref. [13] for a structural effect in the $\Sigma 19a$ grain boundary with apparently contradictory results for the $\Sigma 5$ grain boundary in ref. [15] by new calculations of the latter which serve to reinforce the conclusions reached in ref. [13]. We believe the grain boundary studied in ref. [15] was not in fact embrittled.

In our view the notion that metallic bonds may be either weakened or strengthened by charge transfer is not tenable. Confusion has arisen because calculations supporting these arguments were done using *clusters* of atoms,^{8,62} the effects of screening by the metallic electron gas were thereby excluded;^{11,63} furthermore total energies were not calculated. We do not on the other hand reject chemical effects, but as we have shown these *strengthen* not weaken a grain boundary, at least in the case of substitutional impurities and when defined as here with respect to insertion into a vacant site as opposed to replacement by a host atom.

2. Our second aim was to unfold the complex character of embrittlement by dividing the phenomenon

into independent constituents defined so that for any “cause of embrittlement” there exists a satisfactory thought experiment that isolates it. We then proceed to assess in terms of our numerical data which of these constituents plays the more prominent role.

Our main conclusions can be summarised as follows.

1. Segregation of Bi to the $\Sigma 5$ Cu grain boundary leads to a reduction in its work of separation. We predict that at least a monolayer will segregate resulting in a ductile to brittle transition.
2. We also predict Na to be nearly as good an embrittler as Bi. A striking similarity between the embrittling propensity of free electron metal Na and semi metallic Bi is strong evidence that the embrittlement is primarily a structural effect.
3. Ag is shown not to embrittle the grain boundary, in agreement with experiment. In fact at 0.5 ML it acts as a modest cohesion enhancer at the $\Sigma 5$ grain boundary. This is really a size effect: the larger Ag atom fits well into the “loose site” at the $\Sigma 5$ grain boundary.
4. We suggest an unambiguous, if not unique, thought experiment applicable to both substitutional and interstitial impurities, which allows one to quantify contributions to the changes in W_{sep} coming from the following sources: (*i*) depletion in the interface region (surface or grain boundary) of host atoms (for substitutional impurities only); (*ii*) stretching of the host–host bonds at the interface; and (*iii*) insertion of the impurity into an empty site of pre-stretched interface.

We find the first mechanism to be mostly responsible for the reduction of the work of separation of the boundary with 0.5 ML of Bi or Na. At 1 ML the boundary becomes brittle due to the combined action of the first two mechanisms, whereas the third mechanism acts in the opposite sense.

Acknowledgement

We would like to thank Rainer Schweinfest for discussions and unpublished results. AYL has benefited from discussions with Ruth Lynden-Bell, Pietro Ballone, and Ali Alavi. We acknowledge Malachy Montgomery for computer system management. The work was supported by EPSRC and Invest Northern Ireland.

* Present address: Department of Materials, Imperial College of Science, Technology and Medicine, Exhibition Road, London SW7 2AZ, U.K.

¹ W. Hampe, Berg-, Hütten- u. Salinenwesen **23**, 93 (1874).

² C. Blazey, J. Inst. Metals **41**, 353 (1929).

³ D. Calderon, Proc. Inst. Mech. Engrs. **186**, 341 (1972).

⁴ J. L. Gray, Proc. Inst. Mech. Engrs. **186**, 379 (1972).

⁵ M. P. Seah, Proc. R. Soc. Lond. A **349**, 535 (1976).

⁶ M. P. Seah, Acta Metall. **28**, 955 (1980).

⁷ A. P. Sutton and V. Vitek, Acta Metall. **30**, 2011 (1982).

⁸ R. Messmer and C. L. Briant, Acta Metall. **30**, 457 (1982).

⁹ R. Haydock, J. Phys. C **14**, 3807 (1982).

- ¹⁰ L. Goodwin, R. J. Needs, and V. Heine, Phys. Rev. Letters **60**, 2050 (1988).
- ¹¹ L. Goodwin, R. J. Needs, and V. Heine, Phys. Rev. Letters **63**, 2157 (1989).
- ¹² J. S. Braithwaite and P. Rez, Acta Mater. **53**, 2715 (2005).
- ¹³ R. Schweinfest, A. T. Paxton, and M. W. Finnis, Nature (London) **432**, 1008 (2004).
- ¹⁴ D. A. Muller, Ultramicroscopy **78**, 163 (1999).
- ¹⁵ G. Duscher, M. Chisholm, U. Alber, and M. Rühle, Nature Mater. **3**, 621 (2004).
- ¹⁶ J.-S. Wang, In *Interfacial structure, properties and design, - MRS Symposia Proc. No. 122*, eds. W. A. T. Clark M. H. Yoo and C. L. Briant, (Materials Research Society, Pittsburgh, 1989).
- ¹⁷ J. R. Rice and R. Thomson, Phil. Mag. **29**, 73 (1974).
- ¹⁸ J. R. Rice and J.-S. Wang, Mat. Sci. Eng. **A107**, 23 (1989).
- ¹⁹ D. D. Mason, Phil. Mag. A **39**(4), 455 (1979).
- ²⁰ P. M. Anderson and J. R. Rice, Scripta Metall. **20**, 1467 (1986).
- ²¹ J. P. Hirth and J. R. Rice, Metall. Trans. A **11**, 1501 (1980).
- ²² M. W. Finnis, J. Phys.: Condens. Matter **8**, 5811 (1996).
- ²³ A. P. Sutton and R. W. Balluffi, *Interfaces in Crystalline Materials*, Clarendon Press, Oxford (1995).
- ²⁴ B. D. Powell and H. Mykura, Acta Metall. **21**, 1151 (1973).
- ²⁵ W. T. Geng, A. J. Freeman, R. Wu, C. B. Geller, and J. E. Raynolds, Phys. Rev. B **60**, 7149 (1999).
- ²⁶ R. Janisch and C. Elsässer, Phys. Rev. B **67**, 224101 (2003).
- ²⁷ M. Methfessel, M. van Schilfgaard, and R. A. Casali, In *Electronic Structure and Physical Properties of Solids: The Uses of the LMTO Method. Lecture Notes in Physics*, **535**, ed. H. Dreysse, pages 114–147, Springer-Verlag, Berlin (2000).
- ²⁸ U. von Barth and L. Hedin, J. Phys. C **5**, 1629 (1972).
- ²⁹ V. L. Moruzzi, J. F. Janak, and A. R. Williams, *Calculated Electronic Properties of Metals*, Pergamon, New York (1978).
- ³⁰ E. A. Brandes, editor, *Smithells Metals Reference Book*, Butterworths, London ; Boston, 6 edition (1983).
- ³¹ O. Degtyareva, M. I. McMahan, and R. J. Nelmes, High Pressure Res. **24**, 319 (2004).
- ³² C. Kittel, *Introduction to Solid State Physics*, John Wiley and Sons, Inc., New York, seventh edition (1996).
- ³³ G. Simmons and H. Wang, *Single Crystal Elastic Constants and Calculated Aggregate Properties: A Handbook*, MIT Press, Cambridge, MA, 2nd edition (1971).
- ³⁴ R. Schweinfest, A. T. Paxton, and M. W. Finnis, unpublished.
- ³⁵ A. Khein, D.J. Singh, and C.J. Umrigar, Phys. Rev. B **51**(7), 4105 (1995).
- ³⁶ T. Kraft, P. M. Marcus, M. Methfessel, and M. Scheffler, Phys. Rev. B **48**(9), 5886 (1993).
- ³⁷ M. J. Mehl and D. A. Papaconstantopoulos, Phys. Rev. B **54**(7), 4519 (1996).
- ³⁸ X. Gonze, J.-P. Michenaud, and J.-P. Vigneron, Physica Scripta **37**, 785 (1988).
- ³⁹ Y. Mishin, M.J. Mehl, D.A. Papaconstantopoulos, A.F. Voter, and J.D. Kress, Phys. Rev. B **63**, 224106 (2001).
- ⁴⁰ M.R. Sørensen, Y. Mishin, and A.F. Voter, Phys. Rev. B **62**(6), 3658 (2000).
- ⁴¹ M. W. Finnis, Phys. Stat. Sol. (a) **166**, 397 (1998).
- ⁴² A. Y. Lozovoi, A. Alavi, and M. W. Finnis, Comput. Phys. Commun. **137**, 174 (2001).
- ⁴³ M. Methfessel and A.T. Paxton, Phys. Rev. B **40**(6), 3616 (1989).
- ⁴⁴ W. R. Tyson and W. A. Miller, Surf. Sci. **62**, 267 (1977).
- ⁴⁵ U. Alber, H. Müllejans, and M. Rühle, Acta mater. **47**(15), 4047 (1999).
- ⁴⁶ G. Kresse and J. Furthmüller, Phys. Rev. B **54**, 11169 (1996).
- ⁴⁷ G.H. Li and L.D. Zhang, Scripta Metall. Mater. **32**(9), 1335 (1995).
- ⁴⁸ A. M. Donald and L. M. Brown, Acta Metall. **27**, 59 (1979).
- ⁴⁹ W. Sigle, L.-S. Chang, and W. Gust, Phil. Mag. A **82**(8), 1595 (2002).
- ⁵⁰ B. B. Straumal, S. A. Polyakov, and E. J. Mittemeijer, Acta Mater. **54**, 167 (2006).
- ⁵¹ D. McLean, *Grain boundaries in metals*, Clarendon Press, Oxford (1957).
- ⁵² F. Berthier, J. Creuze, R. Tétot, and B. Legrand, Phys. Rev. B **65**, 195413 (2002).
- ⁵³ T. B. Massalski, editor, *Binary Alloy Phase Diagrams*, ASM International, Materials Park, Ohio, 2nd edition (1996).
- ⁵⁴ P. A. Korzhavyi, I. A. Abrikosov, B. Johansson, A. V. Ruban, and H. L. Skriver, Phys. Rev. B **59**, 11693 (1999).
- ⁵⁵ R. Hultgren, P. D. Desai, D. T. Hawkins, M. Gleiser, and K. K. Kelley, *Selected Values of the Thermodynamic Properties of Binary Alloys*, ASM, Metals Park, Ohio (1973).
- ⁵⁶ N. Papanikolaou, R. Zeller, P. H. Dederichs, and N. Stefanou, Phys. Rev. B **55**, 4157 (1997).
- ⁵⁷ W. B. Pearson, *A Handbook of Lattice Spacings and Structures of Metals and Alloys*, Pergamon Press, London (1958).
- ⁵⁸ T. Korhonen, M. J. Puska, and R. M. Nieminen, Phys. Rev. B **51**, 9526 (1995).
- ⁵⁹ B. Drittler, M. Weinert, R. Zeller, and P. H. Dederichs, Solid State Comm. **79**(1), 31 (1991).
- ⁶⁰ H. Ullmaier, editor, *Properties and Interaction of Atomic Defects in Metals and Alloys*, volume 25 of *Landolt-Bornstein, New Series, Group III*, Springer, Berlin (1991).
- ⁶¹ M. H. Kamdar, Prog. Mater. Sci. **15**, 287 (1973).
- ⁶² M. E. Eberhart and D. D. Vvedensky, Phys. Rev. Lett. **58**, 61 (1987).
- ⁶³ M. A. S. Saqi and D. G. Pettifor, Phil. Mag. Letters **56**, 245 (1987).
- ⁶⁴ In the context of our *ab initio* calculations this is achieved by atomistic relaxation and by exploring a limited number of surface adsorption sites—assuming that these lie in the top layer of the surface.
- ⁶⁵ Although the discussion in this section is of a general nature, we employ the language of computer simulations. Thus “supercell” refers to a representative piece of the system periodically repeated in space, “relaxation” denotes minimisation of the internal energy of the system with respect to atomic positions, and so on. (For details see section III).